

Timelike Compton scattering: exclusive photoproduction of lepton pairs

E.R. Berger^{1,a}, M. Diehl^{2,b,*}, B. Pire^{1,c}

¹ CPHT**, École Polytechnique, 91128 Palaiseau, France

² Deutsches Elektronen-Synchrotron DESY, 22603 Hamburg, Germany

Received: 9 October 2001 /

Published online: 5 April 2002 – © Springer-Verlag / Società Italiana di Fisica 2002

Abstract. We investigate the exclusive photoproduction of a heavy timelike photon which decays into a lepton pair, $\gamma p \rightarrow \ell^+ \ell^- p$. This can be seen as the analog of deeply virtual Compton scattering, and we argue that the two processes are complementary for studying generalized parton distributions in the nucleon. In an unpolarized experiment the angular distribution of the leptons readily provides access to the real part of the Compton amplitude. We estimate the possible size of this effect in kinematics where the Compton process should be dominated by quark exchange.

1 Introduction

A considerable amount of theoretical and experimental work is currently being devoted to the study of generalized parton distributions, whose measurement could make important contributions to our understanding of how quarks and gluons assemble themselves to hadrons [1–3]. The theoretically simplest and cleanest of the exclusive processes where these distributions occur is deeply virtual Compton scattering (DVCS), i.e., $\gamma^* p \rightarrow \gamma p$ in kinematics where the γ^* has large spacelike virtuality while the invariant momentum transfer t to the proton is small. In the present paper, we investigate the “inverse” process, $\gamma p \rightarrow \gamma^* p$ at small t and large *timelike* virtuality of the final state photon. We shall refer to this as timelike Compton scattering (TCS). This reaction shares many features of DVCS, although the timelike character of the virtual photon entails some specific differences. The combination of data on DVCS and TCS would offer a powerful tool to make sure we understand the reaction mechanism, and eventually to obtain stronger constraints on the generalized parton distributions than DVCS alone would provide.

The physical process where to observe TCS is photoproduction of a heavy lepton pair, $\gamma p \rightarrow \mu^+ \mu^- p$ or $\gamma p \rightarrow e^+ e^- p$, shown in Fig. 1. Despite the close analogy to real photon production $ep \rightarrow e\gamma p$ or $\mu p \rightarrow \mu\gamma p$, where DVCS can be accessed, the phenomenology of these reactions shows important differences. In both cases, a

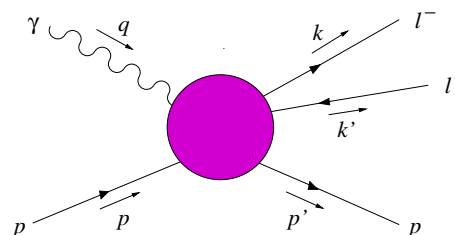


Fig. 1. Real photon–proton scattering into a lepton pair and a proton. ℓ stands for an electron or a muon

Bethe–Heitler (BH) mechanism contributes at the amplitude level. Contrary to the case of DVCS, this contribution *always* dominates over the one from TCS in the kinematical regime where we want to study it. On the other hand, the interference between the TCS and BH processes can readily be accessed through the angular distribution of the lepton pair, whereas the corresponding observable for DVCS is the lepton charge asymmetry and requires beams of both positive and negative charge.

This paper is organized as follows. In Sect. 2 we review the kinematics, factorization properties, and helicity structure of the Compton amplitude in the general case where the two photon virtualities are different, but at least one of them is sufficiently large to provide a hard scale. In Sect. 3 we discuss specific features related to the timelike nature of the outgoing photon in TCS. We develop the phenomenology of exclusive photoproduction of a lepton pair in Sect. 4, taking into account the Bethe–Heitler and the Compton processes and their interference. In Sect. 5 we present estimates of cross sections and of asymmetries suitable to extract information on the Compton signal. Section 6 contains our conclusions. In an appendix we dis-

^a e-mail: edgar.berger@cpht.polytechnique.fr

^b e-mail: markus.diehl@desy.de

^c e-mail: bernard.pire@cpht.polytechnique.fr

* Present address: Institut für Theoretische Physik E, RWTH Aachen, 52056 Aachen, Germany

** Unité mixte C7644 du CNRS

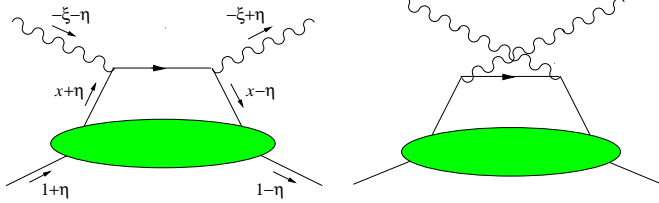


Fig. 2. Handbag diagrams for the Compton process (1) in the scaling limit. The plus-momentum fractions x , ξ , η refer to the average proton momentum $(1/2)(p + p')$

Discuss the relevance of parton densities at very small x when modeling generalized parton distributions with a double distribution ansatz.

2 The Compton amplitude

Both DVCS and TCS are limiting cases of the general Compton process

$$\gamma^*(q) + p(p) \rightarrow \gamma^*(q') + p(p'), \quad (1)$$

where the four-momenta q and q' of the photons can have any virtuality. We will also use $\Delta = p' - p$, the invariants

$$Q^2 = -q^2, \quad Q'^2 = q'^2, \quad s = (p + q)^2, \quad t = \Delta^2, \quad (2)$$

and write M for the proton mass. In the region where at least one of the virtualities is large, the amplitude is given by the convolution of hard scattering coefficients, calculable in perturbation theory, and generalized parton distributions, which describe the nonperturbative physics of the process. To leading order in α_s one then has the quark handbag diagrams of Fig. 2. The arguments for factorization given in [4], based on the analysis of Feynman graphs, hold both for large spacelike and for large timelike virtualities [5]. We thus define the scaling limit as $|q^2| + |q'^2| \rightarrow \infty$ at fixed t and fixed ratios q^2/s and q'^2/s .

For our subsequent discussion let us recall the expression of the hadronic tensor

$$T^{\alpha\beta} = i \int d^4x e^{-iq \cdot x} \langle p(p') | T J_{\text{em}}^\alpha(x) J_{\text{em}}^\beta(0) | p(p) \rangle, \quad (3)$$

where $eJ_{\text{em}}^\alpha(x)$ is the electromagnetic current with e denoting the positron charge. In the scaling limit we have to leading order in α_s

$$T^{\alpha\beta} = -\frac{1}{(p + p')^+} \bar{u}(p') \left[g_{\text{T}}^{\alpha\beta} \left(\mathcal{H}_1 \gamma^+ + \mathcal{E}_1 \frac{i\sigma^{+\rho} \Delta_\rho}{2M} \right) + i\epsilon_{\text{T}}^{\alpha\beta} \left(\tilde{\mathcal{H}}_1 \gamma^+ \gamma_5 + \tilde{\mathcal{E}}_1 \frac{\Delta^+ \gamma_5}{2M} \right) \right] u(p). \quad (4)$$

This expression holds in reference frames where both proton momenta p and p' have small transverse components of order $(-t)^{1/2}$ and are moving fast to the right, i.e., have large plus-components. Light-cone coordinates are defined as $v^\pm = (v^0 \pm v^3)/2^{1/2}$ for any four-vector v . The transverse tensors g_{T} and ϵ_{T} have as only nonzero components

$-g_{\text{T}}^{11} = -g_{\text{T}}^{22} = \epsilon_{\text{T}}^{12} = -\epsilon_{\text{T}}^{21} = 1$. Following the notation of [6] we have introduced the convolutions

$$\begin{aligned} \mathcal{H}_1(\xi, \eta, t) &= \sum_q e_q^2 \int_{-1}^1 dx \left(\frac{H^q(x, \eta, t)}{\xi - x - i\epsilon} - \frac{H^q(x, \eta, t)}{\xi + x - i\epsilon} \right), \\ \mathcal{E}_1(\xi, \eta, t) &= \sum_q e_q^2 \int_{-1}^1 dx \left(\frac{E^q(x, \eta, t)}{\xi - x - i\epsilon} - \frac{E^q(x, \eta, t)}{\xi + x - i\epsilon} \right), \\ \tilde{\mathcal{H}}_1(\xi, \eta, t) &= \sum_q e_q^2 \int_{-1}^1 dx \left(\frac{\tilde{H}^q(x, \eta, t)}{\xi - x - i\epsilon} + \frac{\tilde{H}^q(x, \eta, t)}{\xi + x - i\epsilon} \right), \\ \tilde{\mathcal{E}}_1(\xi, \eta, t) &= \sum_q e_q^2 \int_{-1}^1 dx \left(\frac{\tilde{E}^q(x, \eta, t)}{\xi - x - i\epsilon} + \frac{\tilde{E}^q(x, \eta, t)}{\xi + x - i\epsilon} \right) \end{aligned} \quad (5)$$

of the generalized quark distributions defined in [2], summed over quarks of flavor q and electric charge ee_q . The scaling variables ξ and η are given by

$$\begin{aligned} \xi &= -\frac{(q + q')^2}{2(p + p') \cdot (q + q')} \approx \frac{Q^2 - Q'^2}{2s + Q^2 - Q'^2}, \\ \eta &= -\frac{(q - q') \cdot (q + q')}{(p + p') \cdot (q + q')} \approx \frac{Q^2 + Q'^2}{2s + Q^2 - Q'^2}, \end{aligned} \quad (6)$$

where the approximations hold in the kinematical limit we are working in. x , ξ , and η represent plus-momentum fractions

$$x = \frac{(k + k')^+}{(p + p')^+}, \quad \xi \approx -\frac{(q + q')^+}{(p + p')^+}, \quad \eta \approx \frac{(p - p')^+}{(p + p')^+}. \quad (7)$$

The expressions (4) and (5) reveal that the two-photon amplitude is independent of the photon virtualities at fixed ξ , η and t . In the case of spacelike $q = q'$ this is just Bjorken scaling. To be precise, the independence on q^2 and q'^2 only holds up to logarithmic corrections: the photon virtualities provide the hard scale of the process and thus enter through the factorization scale dependence of the parton distributions, which we have not displayed above. The corresponding evolution equations are well known [1–3, ?], and as usual we will refer to $-1 < x < -\eta$ and $\eta < x < 1$ as the DGLAP regions, and to $-\eta < x < \eta$ as the ERBL region of the parton distributions.

Let us now recall the helicity structure of the two-photon process in the scaling limit. Contracting the hadronic tensor with polarization vectors ϵ of the incoming and ϵ' of the outgoing photon, one obtains the helicity amplitudes of (1) as

$$e^2 M^{\lambda' \mu', \lambda \mu} = e^2 \epsilon_\alpha T^{\alpha\beta} \epsilon_\beta'^*, \quad (8)$$

where λ (λ') denotes the helicity of the incoming (outgoing) proton and μ (μ') the helicity of the incoming (outgoing) photon. Parity invariance provides the relations $M^{-\lambda' - \mu', -\lambda - \mu} = (-1)^{\lambda' - \mu' - \lambda + \mu} M^{\lambda' \mu', \lambda \mu}$. From (4) one easily finds that the quark handbag diagrams only generate helicity conserving transitions between transverse photons, $M^{\lambda' +, \lambda +}$ and $M^{\lambda' -, \lambda -}$. At order α_s one further has

amplitudes $M^{\lambda'0,\lambda 0}$, provided of course that both photons are off shell [8]. Double helicity flip amplitudes $M^{\lambda'+,\lambda-}$ and $M^{\lambda'-,\lambda+}$ are generated at order α_s by gluon transversity distributions [9,10]. Finally, transitions involving one transverse and one longitudinal photon are suppressed by one power of the large scale Q or Q' . These twist-three contributions¹ have been studied in [11], and twist-four contributions to the double helicity flip amplitudes in [12]. These studies were performed for large spacelike virtualities; whether they can be extended to the timelike case is a question beyond the scope of this paper.

The DVCS and TCS processes are limiting cases of (1) where one of the photons is on shell. From (6) we readily see that to leading-twist accuracy one has $\xi = \eta$ in DVCS and $\xi = -\eta$ in TCS. The convolutions (5) obey

$$\begin{aligned}\mathcal{H}_1(-\eta, \eta, t) &= [\mathcal{H}_1(\eta, \eta, t)]^*, \\ \tilde{\mathcal{H}}_1(-\eta, \eta, t) &= -[\tilde{\mathcal{H}}_1(\eta, \eta, t)]^*, \\ \mathcal{E}_1(-\eta, \eta, t) &= [\mathcal{E}_1(\eta, \eta, t)]^*, \\ \tilde{\mathcal{E}}_1(-\eta, \eta, t) &= -[\tilde{\mathcal{E}}_1(\eta, \eta, t)]^*,\end{aligned}\quad (9)$$

which leads to the simple relations

$$\begin{aligned}M^{\lambda'+,\lambda+}\Big|_{\text{TCS}} &= [M^{\lambda'-,\lambda-}]_{\text{DVCS}}^*, \\ M^{\lambda'-,\lambda-}\Big|_{\text{TCS}} &= [M^{\lambda'+,\lambda+}]_{\text{DVCS}}^*\end{aligned}\quad (10)$$

between the helicity amplitudes for TCS and DVCS at equal values of η and t . These relations should be evaluated at corresponding values of Q'^2 and Q^2 since the photon virtualities play analogous roles in providing the hard scale of the respective processes and thus enter in the scale dependence of the parton distributions. The relations (10) tell us that at Born level and to leading twist one obtains the amplitudes for TCS from those of DVCS by changing the sign of the imaginary part and reversing the photon polarizations. To this accuracy, the two processes thus carry exactly the same information on the generalized quark distributions.

We remark that the relations (9) and hence (10) no longer hold at $O(\alpha_s)$, neither for the one-loop corrections to the quark handbag diagrams in Fig. 2 nor for the diagrams involving gluon distributions. On general grounds, the phase structure of the two processes is in fact different. Whereas the only discontinuity of the two-photon amplitude in DVCS kinematics is in the s -channel, the TCS amplitude has discontinuities in both s and Q'^2 , with one-loop hard scattering diagrams contributing to both cuts. In situations where $O(\alpha_s)$ contributions are important, the DVCS and TCS processes will have a different dependence on the generalized parton distributions. TCS and DVCS together can then constrain them more effectively than either process alone. The detailed study of TCS at one-loop level is beyond the scope of this work, and we will base our numerical studies on the Born level expression (4).

¹ We use here the dynamical definition of twist, where twist n contributions to the Compton amplitude are suppressed by $n - 2$ inverse powers of the large scale

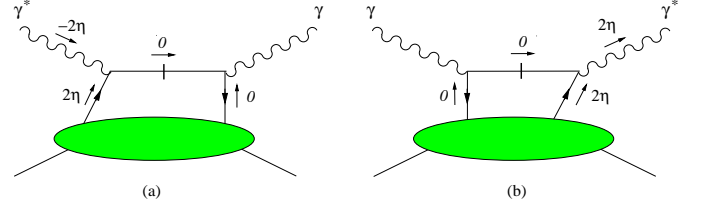


Fig. 3a,b. The loop momentum configurations $x = \eta$ where the Born level amplitude receives its imaginary part in **a** DVCS and **b** TCS. Short vertical lines indicate on-shell quark lines in the hard scattering, plus-momentum fractions $\pm 2\eta$ and 0 refer to the average proton momentum $(1/2)(p + p')$. The corresponding configurations for $x = -\eta$ are obtained by reversing the charge flow of the quark line

It is worthwhile to compare the momentum configurations in DVCS and TCS from which the Born level convolutions (5) receive their imaginary parts. From Fig. 3 we see that in both cases there is a quark line with zero plus-momentum coming from the proton, and that in both cases it is attached to the real photon, i.e., to the final state in DVCS and to the initial state in TCS.

We conclude this section by defining the variable

$$\tau = \frac{Q'^2}{2p \cdot q} = \frac{Q'^2}{s - M^2} \quad (11)$$

for the TCS process as the analog of the Bjorken variable $x_B = Q^2/(2p \cdot q)$ in DVCS. The similar roles played by these quantities reveals itself in their relations with η , which to leading-twist accuracy reads $\eta = \tau/(2 - \tau)$ for TCS and $\eta = x_B/(2 - x_B)$ for DVCS.

3 The timelike photon

Processes involving timelike photons can have markedly different features than processes controlled by large spacelike virtualities. These features usually do not arise to leading order in perturbation theory, which is the approximation we will work in here. A closer look at the Born level diagrams reveals nevertheless important similarities and differences between timelike processes, which we now briefly discuss.

The reaction which at first sight is most similar to TCS is Drell–Yan pair production in hadron–hadron collisions. In that case, the $O(\alpha_s)$ corrections to the Born graph of Fig. 4a have considerable size and make up for most of the much discussed K -factor of this process. A way to understand them is the occurrence of large contributions enhanced by π^2 , which can be traced back to the correction of the quark-photon vertex for spacelike γ^* and on-shell quarks [13]. Notice that in the TCS Born graphs of Fig. 2 only one of the two quark lines attached to the γ^* is on shell, whereas the other one is off shell by order Q'^2 . One might argue that the second line does become on shell in the imaginary part of the amplitude, as indicated in Fig. 3b, but there is an important difference: the quark lines in the Drell–Yan diagram and one of the lines

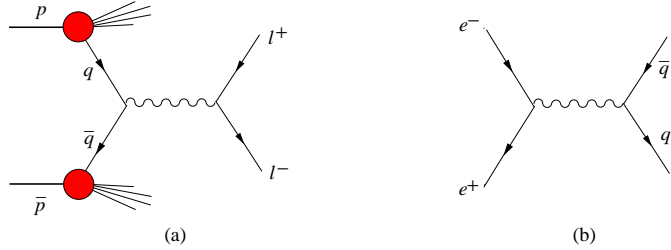


Fig. 4a,b. Born level diagrams for the **a** Drell–Yan process $p\bar{p} \rightarrow \ell^+\ell^-X$ and **b** e^+e^- annihilation into hadrons, $e^+e^- \rightarrow X$

in TCS physically correspond to small virtualities as they are directly attached to parton distributions, i.e., to quantities describing long-distance physics. This is not the case for the vertical quark line in the TCS diagrams. Technically, the singularity of its propagator can be avoided by analytical continuation of the loop momenta, whereas the singularities associated with the lines attached to a parton distribution are pinched [4,14]. The analogy between the two processes must hence be used with care, and in particular one cannot easily infer on the size of the $O(\alpha_s)$ corrections from the experience with the Drell–Yan process.

A second issue in processes with timelike photons is the importance of resonance effects, which are beyond the realm of perturbation theory. At invariant photon masses above 4 or 5 GeV, excluding of course the region of the Υ resonances, the comparison of leading-twist perturbative calculations and data works rather satisfactorily for the Drell–Yan process, cf. the data compilation in [15]. The situation for masses below the J/Ψ is difficult to assess, mainly due to background lepton pairs from the weak decays of b and c quarks [16]. This type of background does of course not affect TCS, where we are dealing with *exclusive* lepton pair production. As for inclusive e^+e^- annihilation into hadrons, the recent BES data [17] in the mass region from 2 to 3 GeV is remarkably flat and close to the leading-twist result. The same holds for the data above 5 GeV, cf. e.g. [18], excluding again the Υ region. Between 3 and 5 GeV on the other hand, resonance structures are clearly visible [17].

Again one should keep in mind that the importance of resonance effects may be different in all these processes. In line with our above analysis, we remark that in the tree level diagram for inclusive e^+e^- annihilation, Fig. 4b, both quark and antiquark correspond to large virtualities. Technically, the cross section is calculated as the imaginary part of the photon vacuum polarization, where the quarks appear in a loop and are indeed far off shell. We notice that in both Drell–Yan production and e^+e^- annihilation one has quark–antiquark configurations with comparable virtualities. In contrast, we have asymmetric configurations in TCS, with one quark line soft and the other far off shell. Furthermore, the space-time structure of TCS is such that the γ^* is formed from a $q\bar{q}$ -pair only in the ERLB region of the parton distributions, while in the DGLAP region the parton-level process is photon radiation off a quark or antiquark, $q \rightarrow \gamma^*q$ or $\bar{q} \rightarrow \gamma^*\bar{q}$.

To conclude, we estimate based on $e^+e^- \rightarrow X$ and the Drell–Yan data that ranges of Q' where the leading-twist description of TCS may work should be between about 1.5 to 2 GeV and the J/Ψ mass, and above the charmonium resonances. We stress however that the reaction mechanism in the TCS process displays important differences, and that one will have to see in the data how parton–hadron duality manifests itself here.

4 Observing TCS in lepton pair production

4.1 Some kinematics

Let us now specify the variables we use to describe the lepton pair production process depicted in Fig. 1, in addition to those already introduced at the beginning of Sect. 2. A useful quantity is the transverse component $\vec{\Delta}_T$ of the momentum transfer Δ with respect to \vec{p} and \vec{q} in the γp c.m. It is related to the scattering angle Θ_{cm} in that frame by

$$\sin \Theta_{\text{cm}} = \frac{2\Delta_T \sqrt{s}}{r}, \quad (12)$$

where $\Delta_T = |\vec{\Delta}_T|$ and $r = ((s - Q'^2 - M^2)^2 - 4Q'^2 M^2)^{1/2}$. In the limit of large Q'^2 , large s , and small $-t$, we then have

$$-t \approx \frac{\tau^2 M^2 + \Delta_T^2}{1 - \tau} \quad (13)$$

up to relative corrections of order M^2/Q'^2 . For the lepton pair, we use the lepton velocity

$$\beta = \sqrt{1 - 4m_\ell^2/Q'^2} \quad (14)$$

in the $\ell^+\ell^-$ c.m., where m_ℓ denotes the lepton mass. In the same frame we introduce the polar and azimuthal angles θ and φ of \vec{k} , with reference to a coordinate system with 3-axis along $-\vec{p}'$ and 1- and 2-axes such that \vec{p} lies in the 1–3 plane and has a positive 1-component². This is shown in Fig. 5. In terms of Lorentz invariants, our angles are given by

$$2(k - k') \cdot p' = \beta r \cos \theta, \quad (15)$$

$$2(k - k') \cdot (p - p') = -\beta \frac{2(s - M^2)Q' \Delta_T}{r} \sin \theta \cos \varphi$$

$$+\sigma \beta \sqrt{(Q'^2 - t)^2 - \left[\frac{2(s - M^2)Q' \Delta_T}{r} \right]^2} \cos \theta,$$

$$4\epsilon^{\mu\nu\rho\sigma} p_\mu p'_\nu k_\rho k'_\sigma = \beta(s - M^2)Q' \Delta_T \sin \theta \sin \varphi,$$

where our convention for the completely antisymmetric tensor is $\epsilon_{0123} = 1$, and the sign factor $\sigma = \pm 1$ is determined by

$$\sigma \sqrt{(Q'^2 - t)^2 - \left[\frac{2(s - M^2)Q' \Delta_T}{r} \right]^2}$$

² They correspond to the decay angles θ and ϕ for vector meson photoproduction introduced by Schilling, Seyboth and Wolf [19] with their vector $\vec{\pi}$ along \vec{k}

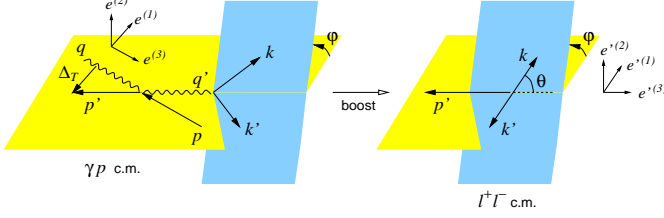


Fig. 5. Sketch of the kinematical variables and coordinate axes in the γp and $\ell^+ \ell^-$ c.m. frames. Notice that the coordinate systems differ from the one we used in the Compton amplitude (4), where p and p' have positive 3-components

$$= \frac{Q'^2(s - M^2 - Q'^2) + t(s - M^2 + Q'^2)}{r}. \quad (16)$$

The form of the second equation in (15) is useful in our kinematics, where Δ_T is small and $\sigma = 1$.

As polarization vectors $\epsilon(\lambda)$ for the incoming photon we take $\epsilon(\pm) = (\mp e^{(1)} - i e^{(2)})/2^{1/2}$, where $e^{(1)}$ and $e^{(2)}$ are unit vectors along the 1- and 2-directions in the γp c.m. as shown in Fig. 5. Our polarizations $\epsilon'(\lambda')$ of the outgoing photon are $\epsilon'(\pm) = (\mp e'^{(1)} - i e'^{(2)})/2^{1/2}$ and $\epsilon'(0) = e'^{(3)}$ with unit vectors along the coordinate axes in the $\ell^+ \ell^-$ c.m. described above.

4.2 The Bethe–Heitler contribution

The Bethe–Heitler amplitude is readily calculated from the two Feynman diagrams in Fig. 6. We parameterize the photon–proton vertex in terms of the usual Dirac and Pauli form factors $F_1(t)$ and $F_2(t)$, normalizing $F_2(0)$ to be the anomalous magnetic moment of the target. We find for the BH contribution to the unpolarized γp cross section

$$\frac{d\sigma_{\text{BH}}}{dQ'^2 dt d(\cos\theta) d\varphi} = \frac{\alpha_{\text{em}}^3}{4\pi(s - M^2)^2} \frac{\beta}{-tL} \times \left[\left(F_1^2 - \frac{t}{4M^2} F_2^2 \right) \frac{A}{-t} + (F_1 + F_2)^2 \frac{B}{2} \right], \quad (17)$$

where we have used the abbreviations

$$\begin{aligned} A &= (s - M^2)^2 \Delta_T^2 - ta(a + b) \\ &\quad - M^2 b^2 - t(4M^2 - t)Q'^2 \\ &\quad + \frac{m_\ell^2}{L} [\{(Q'^2 - t)(a + b) - (s - M^2)b\}^2 \\ &\quad + t(4M^2 - t)(Q'^2 - t)^2], \\ B &= (Q'^2 + t)^2 + b^2 \\ &\quad + 8m_\ell^2 Q'^2 - \frac{4m_\ell^2(t + 2m_\ell^2)}{L} (Q'^2 - t)^2. \end{aligned} \quad (18)$$

The cross section depends on the angles θ and φ through the scalar products

$$a = 2(k - k') \cdot p', \quad b = 2(k - k') \cdot (p - p') \quad (19)$$

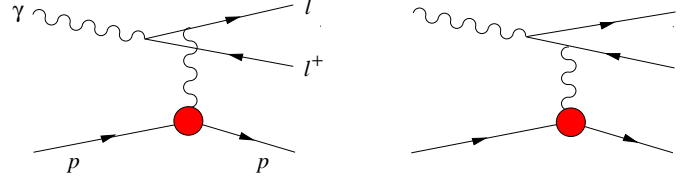


Fig. 6. The Feynman diagrams for the Bethe–Heitler amplitude

given in (15) above, and through the product of the lepton propagators in the two BH diagrams,

$$L = [(q - k)^2 - m_\ell^2][(q - k')^2 - m_\ell^2] = \frac{(Q'^2 - t)^2 - b^2}{4}. \quad (20)$$

These expressions are rather lengthy, but simplify considerably in kinematics where t , M^2 and m_ℓ^2 can be neglected compared to terms going with s or Q'^2 . We then have

$$L \approx L_0 = \frac{Q'^4 \sin^2 \theta}{4}. \quad (21)$$

and

$$\begin{aligned} \frac{d\sigma_{\text{BH}}}{dQ'^2 dt d(\cos\theta) d\varphi} &\approx \frac{\alpha_{\text{em}}^3}{2\pi s^2} \frac{1}{-t} \frac{1 + \cos^2 \theta}{\sin^2 \theta} \\ &\times \left[\left(F_1^2 - \frac{t}{4M^2} F_2^2 \right) \frac{2}{\tau^2} \frac{\Delta_T^2}{-t} + (F_1 + F_2)^2 \right]. \end{aligned} \quad (22)$$

We see that the product L of lepton propagators goes to zero at $\sin\theta = 0$ in this approximation. Closer inspection reveals that when $\sin\theta$ becomes of order Δ_T/Q' or m_ℓ/Q' the approximations (21) and (22) break down and one must use the full expressions.

Let us see how small the product L can become. At fixed s , Q'^2 , t , φ we find with (15) and (20) that L assumes a minimum value,

$$L_{\text{min}} \approx Q'^2 m_\ell^2 + Q'^2 \Delta_T^2 \frac{\sin^2 \varphi}{(1 - \tau)^2}, \quad (23)$$

for

$$\tan \theta_{\text{min}} \approx -\frac{2\Delta_T \cos \varphi}{Q' (1 - \tau)}, \quad (24)$$

up to corrections of order t/Q'^2 , M^2/Q'^2 , m_ℓ^2/Q'^2 . For $\theta \sim \theta_{\text{min}}$ the leptons ℓ^- and ℓ^+ are nearly collinear with the initial photon in the γp c.m. They have transverse momenta of order Δ_T with respect to \vec{p} and \vec{q} and share their total longitudinal momentum in a highly asymmetric way. In our numerical studies we will impose a cut on θ which ensures that L remains of order Q'^4 , thus staying away from the region where the BH cross section becomes extremely large.

We finally remark that as long as L is of order Q'^4 the terms going with $1/L$ in (18) are suppressed at least like $m_\ell^2 Q'^2/L$ compared with the leading behavior of A and B . For a large range in θ the BH cross section (17) will thus approximately behave like $1/L$ instead of $1/L^2$.

4.3 The Compton scattering contribution

We now investigate the TCS contribution to lepton pair production. In order to understand the basics of its interplay with the BH process it is sufficient to consider the leading behavior of the Compton amplitude in $1/Q'$ and in α_s , which we discussed in Sect. 2. We will thus in particular discard γp amplitudes that change the photon helicity. In line with neglecting power suppressed effects in the Compton subprocess we will also drop mass corrections of order M^2/Q'^2 and m_ℓ^2/Q'^2 in kinematics and phase space. To this accuracy, the contribution of TCS to the unpolarized cross section of $\gamma p \rightarrow \ell^+ \ell^- p$ reads

$$\frac{d\sigma_{\text{TCS}}}{dQ'^2 dt d(\cos\theta) d\varphi} \approx \frac{\alpha_{\text{em}}^3}{8\pi s^2} \frac{1}{Q'^2} \frac{1 + \cos^2\theta}{4} \sum_{\lambda, \lambda'} |M^{\lambda', \lambda-}|^2. \quad (25)$$

We note that the φ independence here is a consequence of having neglected photon helicity changing transitions. From (4) we obtain

$$\begin{aligned} \frac{1}{2} \sum_{\lambda, \lambda'} |M^{\lambda', \lambda-}|^2 &= (1 - \eta^2) (|\mathcal{H}_1|^2 + |\tilde{\mathcal{H}}_1|^2) \\ &- 2\eta^2 \text{Re}(\mathcal{H}_1^* \mathcal{E}_1 + \tilde{\mathcal{H}}_1^* \tilde{\mathcal{E}}_1) \\ &- \left(\eta^2 + \frac{t}{4M^2} \right) |\mathcal{E}_1|^2 - \eta^2 \frac{t}{4M^2} |\tilde{\mathcal{E}}_1|^2, \end{aligned} \quad (26)$$

where \mathcal{H}_1 , $\tilde{\mathcal{H}}_1$, \mathcal{E}_1 , $\tilde{\mathcal{E}}_1$ are to be evaluated at $-\xi = \eta$. Together with (22) we see that compared with the TCS cross section, the BH contribution is parametrically enhanced by a factor $Q'^2/(-t)$ and has an extra factor of $1/\sin^2\theta$ in the angular dependence.

Let us compare the TCS result (25) with the contribution of DVCS to the electroproduction process

$$\ell(k) + p(p) \rightarrow \ell(k') + \gamma(q') + p(p'), \quad (27)$$

where we have indicated four-momenta in parentheses. Retaining only the leading part in $1/Q$ and α_s of the Compton amplitude, and dropping again mass corrections of order M^2/Q^2 and m_ℓ^2/Q^2 , we have for the unpolarized cross section

$$\frac{d\sigma_{\text{DVCS}}}{dQ^2 dt dy d\varphi} \approx \frac{\alpha_{\text{em}}^3}{8\pi s_{ep}^2} \frac{1}{Q^2} \frac{1 + (1-y)^2}{y^3} \sum_{\lambda, \lambda'} |M^{\lambda', \lambda+}|^2. \quad (28)$$

Here $s_{ep} = (p+k)^2$ is the total c.m. energy of the ep collision, $y = (q \cdot p)/(k \cdot p)$ the usual inelasticity parameter, and φ the azimuthal angle between lepton and hadron planes as defined in [9]. With the relation (10) we readily see that to leading twist and leading order in α_s the sums over squared helicity amplitudes in (25) and (28) give identical results for corresponding values of $\eta = \tau/(2 - \tau)$ and Q'^2 in TCS, and $\eta = x_B/(2 - x_B)$ and Q^2 in DVCS. To this accuracy, the Compton scattering contributions to the respective cross sections only differ by the global kinematic factors given in (25) and (28).

Comparison of these factors reveals the correspondence between the variables θ in TCS and y in DVCS, which by expressing them in terms of scalar products is found to be

$$\frac{1 + \cos\theta}{2} \approx \frac{k \cdot p'}{(k + k') \cdot p'} \leftrightarrow \frac{k \cdot p}{(k - k') \cdot p} = \frac{1}{y}, \quad (29)$$

where in the first relation we have again neglected mass corrections. At this point we find a crucial difference in the phenomenology of the two processes. As is well known [9, 20] the relative weight of DVCS and BH crucially depends on y , given that at amplitude level the DVCS contribution comes with a factor $1/y$ relative to the BH contribution. In the region of Q^2 and t defining the DVCS regime, BH dominates for moderate values of y , whereas for sufficiently small values of y the Compton contribution wins. Since the quantity corresponding to $1/y$ in (29) is always between -1 and 1 , no such enhancement takes place for TCS, and we will indeed find numerically that here the BH contribution to the cross section is always dominant. The strategy is then the same as in DVCS at moderate values of y , namely to gain information on the Compton process through its interference with BH, which can be extracted using symmetry properties of the process.

Another noteworthy difference concerns the variables τ and x_B , which determine the values η where the generalized parton distributions are probed in the two processes. In DVCS at fixed collision energy $s_{ep}^{1/2}$ the variables x_B and y are not independent since $Q^2 = y x_B (s_{ep} - m_\ell^2 - M^2)$. If at given Q^2 one wants to vary x_B and thus choose a kinematical point where to probe the Compton subprocess, one must vary y . In TCS on the other hand, one has the relation $Q'^2 = \tau(s - M^2)$, independent of the value of θ . In order to vary τ at given Q'^2 , one here needs to change the γp collision energy $s^{1/2}$. A continuous spectrum in s is of course automatically obtained if the initial photon originates from bremsstrahlung off a lepton beam.

4.4 The interference term

Let us now explore how information on the Compton process can be obtained from the interference between the TCS and BH amplitudes. The general strategy is the same as described in [9] for the case of DVCS, but we will again encounter important differences in the phenomenology of these reactions.

A key point is that the amplitudes for the Compton and Bethe-Heitler processes transform with opposite signs under reversal of the lepton charge. As a consequence the interference term between TCS and BH is odd under exchange of the ℓ^+ and ℓ^- momenta, whereas the individual contributions of the two processes are even. Any observable that changes sign under $k \leftrightarrow k'$ will hence project out the interference term, eliminating in particular the large BH contribution. Clean information on the interference term is therefore contained in the angular distribution of the lepton pair. The corresponding observable in the electroproduction process $\ell p \rightarrow \ell \gamma p$ is the lepton beam charge asymmetry, whose measurement presents important experimental challenges.

Let us take a closer look at the interference part of the cross section for $\gamma p \rightarrow \ell^+ \ell^- p$ with unpolarized protons and photons. It is given by

$$\begin{aligned} \frac{d\sigma_{\text{INT}}}{dQ'^2 dt d(\cos\theta) d\varphi} &= -\frac{\alpha_{\text{em}}^3}{4\pi s^2} \frac{1}{-t} \frac{M}{Q'} \frac{1}{\tau\sqrt{1-\tau}} \frac{L_0}{L} \\ &\times \left[\cos\varphi \frac{1+\cos^2\theta}{\sin\theta} \text{Re}\tilde{M}^{--} - \cos 2\varphi\sqrt{2} \cos\theta \text{Re}\tilde{M}^{0-} \right. \\ &\left. + \cos 3\varphi \sin\theta \text{Re}\tilde{M}^{+-} + O\left(\frac{1}{Q'}\right) \right], \end{aligned} \quad (30)$$

with L and L_0 from (20) and (21). Here

$$\begin{aligned} \tilde{M}^{\mu'\mu} &= \frac{\Delta_{\text{T}}}{M} \left[(1-\tau)F_1 - \frac{\tau}{2}F_2 \right] M^{-\mu',-\mu} \\ &+ \frac{\Delta_{\text{T}}}{M} \left[F_1 + \frac{\tau}{2}F_2 \right] M^{+\mu',+\mu} \\ &+ \left[\tau^2(F_1+F_2) + \frac{\Delta_{\text{T}}^2}{2M^2}F_2 \right] M^{-\mu',+\mu} \\ &- \frac{\Delta_{\text{T}}^2}{2M^2}F_2 M^{+\mu',-\mu} \end{aligned} \quad (31)$$

is the same combination of Compton helicity amplitudes as defined in [9]³. The close analogy between TCS and DVCS is manifest, and we see that a γ^* with negative helicity in TCS corresponds to a γ^* with positive helicity in DVCS as we already found in the relations (10).

The terms indicated by $O(1/Q')$ in (30) have kinematical coefficients suppressed by at least one power of $1/Q'$ relative to the other terms in brackets. Notice that we have not approximated the product L of lepton propagators from the BH process. In the limit of large Q'^2 the factor L_0/L tends to 1, but we have seen in Sect. 4.2 that this approximation becomes increasingly bad as θ approaches 0 or π , so that it is useful to keep L_0/L in an analysis. The same is true for the lepton propagators in the interference of DVCS and BH, as has been emphasized in [6].

We see that without polarization one probes the real parts of the Compton helicity amplitudes. Access to the imaginary parts can be obtained with polarized photon beams. If the photons have a circular polarization ν , as is the case for a bremsstrahlung beam emitted from longitudinally polarized leptons, one has

$$\begin{aligned} \frac{d\sigma_{\text{INT}}}{dQ'^2 dt d(\cos\theta) d\varphi} &= \frac{d\sigma_{\text{INT}}}{dQ'^2 dt d(\cos\theta) d\varphi} \Big|_{\text{Eq. (30)}} \\ &- \nu \frac{\alpha_{\text{em}}^3}{4\pi s^2} \frac{1}{-t} \frac{M}{Q'} \frac{1}{\tau\sqrt{1-\tau}} \frac{L_0}{L} \\ &\times \left[\sin\varphi \frac{1+\cos^2\theta}{\sin\theta} \text{Im}\tilde{M}^{--} - \sin 2\varphi\sqrt{2} \cos\theta \text{Im}\tilde{M}^{0-} \right. \\ &\left. + \sin 3\varphi \sin\theta \text{Im}\tilde{M}^{+-} + O\left(\frac{1}{Q'}\right) \right]. \end{aligned} \quad (32)$$

³ In contrast to [9] our notation here is to list the helicities of outgoing particles first. With our phase convention the transverse polarization vectors of the two photons coincide for $\Delta_{\text{T}} = 0$, cf. Sect. 4.1. In [9] we made a different choice, and the Compton helicity amplitudes here and there differ by an overall sign

The photon polarization dependent and independent terms are simply related by exchanging $\sin \leftrightarrow \cos$ and $\text{Im} \leftrightarrow \text{Re}$. This is not quite the same as for *lepton* beam polarization in the interference between DVCS and BH, where different kinematical factors occur in the polarization dependent and independent parts, and where notably the term with $\sin 3\varphi \text{Im}\tilde{M}^{+-}$ is absent.

The various terms in the φ dependence of the interference term can for instance be projected out by weighting the differential cross section with appropriate functions. The weights $(L/L_0) \cos(n\varphi)$ and $(L/L_0) \sin(n\varphi)$ for instance give the terms with $\cos(n\varphi)$ and $\sin(n\varphi)$ in (30) and (32), respectively. Notice that these weights are odd under the exchange of k and k' and hence do not pick up the BH and TCS contributions to the cross section, as discussed above.

In this way we can project out the various helicity combinations $\tilde{M}^{\mu'\mu}$ of Compton amplitudes, up to relative corrections in $1/Q'$. Along the lines of [9] this can be used to test whether the power behavior in Q' at fixed τ and t follows the predictions discussed in Sect. 2, i.e., whether arguments based on the large Q'^2 limit apply at the finite Q'^2 of a measurement. If one is in the scaling regime, one can then analyze the photon helicity conserving amplitudes in terms of generalized parton distributions. The quark handbag diagrams of Fig. 2 give

$$\begin{aligned} \tilde{M}^{--} &= \frac{2\sqrt{t_0-t}}{M} \frac{1-\eta}{1+\eta} \\ &\times \left[F_1 \mathcal{H}_1 - \eta(F_1+F_2) \tilde{\mathcal{H}}_1 - \frac{t}{4M^2} F_2 \mathcal{E}_1 \right], \end{aligned} \quad (33)$$

where $-t_0 = 4\eta^2 M^2 / (1-\eta^2)$ is the minimal value of $-t$ at given η , up to corrections in $1/Q'^2$.

The above extraction of the Compton amplitudes requires measurement of the angle φ . If one integrates the interference term over φ , the photon polarization dependent part in (32) vanishes because of parity invariance. The integral of the unpolarized contribution (30) is nonzero, due to the φ dependence of L_0/L and to the φ independent part of the terms denoted by $O(1/Q')$. This integral can in principle be projected out from the cross section because it is odd under $\theta \rightarrow \pi - \theta$, whereas the BH and TCS contributions are even when integrated over φ . The interference signal so obtained is however an order $1/Q'$ smaller than what can be seen in the φ dependence of the cross section, and will thus be harder to extract.

5 Numerical estimates

In this section we model the generalized parton distributions (GPDs) and give estimates for various observables. We restrict ourselves to moderate values of τ and use the leading-order handbag approximation (4), (5) of the Compton amplitude. We omit all terms proportional to E^q and \bar{E}^q . In the region $0.1 \leq \tau \leq 0.36$ and $|t| \leq 0.4 \text{ GeV}^2$ we will consider in our estimates, \mathcal{E}_1 is multiplied by kinematical coefficients at most 0.15 times those of \mathcal{H}_1 in (26)

and (33) and thus would not significantly change our results. In any case, it is at present fairly unclear how to model the distributions E^q , so that taking them into account would not improve the reliability of the estimates. As for $\tilde{\mathcal{E}}_1$, it is multiplied by a tiny coefficient in (26) and absent in the interference term (33).

5.1 Modeling the parton distributions

Now we define the model we use for H^q and \tilde{H}^q . Following [21] we take a factorizing ansatz for the t dependence,

$$\begin{aligned} H_{\text{DD}}^u(x, \eta, t) &= h^u(x, \eta) \frac{1}{2} F_1^u(t), \\ H_{\text{DD}}^d(x, \eta, t) &= h^d(x, \eta) F_1^d(t), \\ \tilde{H}_{\text{DD}}^q(x, \eta, t) &= \tilde{h}^q(x, \eta) \tilde{F}^q(t), \end{aligned} \quad (34)$$

with

$$\begin{aligned} F_1^u(t) &= 2F_1^p(t) + F_1^n(t), \\ F_1^d(t) &= F_1^p(t) + 2F_1^n(t), \\ \tilde{F}^u(t) &= \tilde{F}^d(t) = g_A(t)/g_A(0). \end{aligned} \quad (35)$$

F_1^p and F_1^n are the electromagnetic Dirac form factors of the proton and neutron, for which we take the usual dipole parameterization [22]. For the axial form factor of the proton we take $g_A(t) = g_A(0)(1 - t/M_A^2)^{-2}$ with $g_A(0) = 1.26$ and $M_A = 1.06$ GeV from [23]. For strange quarks we make the ansatz

$$H_{\text{DD}}^s(x, \eta, t) = h^s(x, \eta) F_D(t), \quad (36)$$

where the dipole form factor $F_D(t) = (1 - t/M_V^2)^{-2}$ with $M_V = 0.84$ GeV is the same as the one that enters in the parameterization of F_1^p and F_1^n . Note that via the sum rule for $\int dx H^s(x, \eta, t)$ a factorizing ansatz like (36) corresponds to setting the strange quark contribution $F_1^s(t)$ to the Dirac form factor to zero. We remark that several studies [24, 25] indicate that GPDs do *not* factorize in the simple manner of (34) and (36). The ansatz has however the virtue of simplicity and should be good enough for our estimates, as long as we do not study the interplay of the η and t dependence of the cross section. For h^q and \tilde{h}^q we make an ansatz based on double distributions [26],

$$\begin{aligned} h^q(x, \eta) &= \int_0^1 dx' \int_{-1+x'}^{1-x'} dy' [\delta(x - x' - \eta y') q(x') \\ &\quad - \delta(x + x' - \eta y') \bar{q}(x')] \pi(x', y'), \end{aligned} \quad (37)$$

$$\begin{aligned} \tilde{h}^q(x, \eta) &= \int_0^1 dx' \int_{-1+x'}^{1-x'} dy' \\ &\quad \times \delta(x - x' - \eta y') \Delta q_V(x') \pi(x', y'), \end{aligned} \quad (38)$$

$$\pi(x', y') = \frac{3}{4} \frac{(1 - x')^2 - y'^2}{(1 - x')^3}. \quad (39)$$

We evaluate (37) with the LO GRV 94 parameterization [27] of the unpolarized distributions $q(x)$ and $\bar{q}(x)$, and

(38) with set A of the LO polarized valence distributions $\Delta q_V(x)$ by Gehrman and Stirling [28]. In both cases we take the factorization scale as $\mu^2 = 5$ GeV². We neglect the polarized quark sea, which presently is not well constrained by data, and thereby also drop \tilde{H}^s . In the appendix we shall give a detailed discussion of the role played by very small values of x' in the integrals of (37) and (38), and thus of the uncertainties in evaluating them with parton densities only known above some finite value of x' .

Let us stress that the available models of GPDs are fraught with uncertainties, in particular in the ERBL region. There, GPDs describe the emission of a $q\bar{q}$ -pair from the target, and an ansatz only using the information from usual parton densities should be used with care. Dynamical calculations [29, 24] lead in fact to much richer structure in the ERBL region than is generated from (37) to (39). Notice also that, while for $x > \eta$ GPDs are bounded from above [30], no analogous constraints are known in the ERBL region.

A particular type of contribution in the ERBL region is the Polyakov–Weiss D -term [31], which following [32] we take as a flavor $SU(3)$ singlet:

$$\begin{aligned} H_D^u(x, \eta, t) &= H_D^d(x, \eta, t) = H_D^s(x, \eta, t) \\ &= \Theta(\eta^2 - x^2) \frac{1}{3} D\left(\frac{x}{\eta}\right) F_D(t), \end{aligned} \quad (40)$$

where Θ denotes the step function. We make again a factorizing ansatz for the t dependence, taking the same dipole form factor as in (36). For the function D we use the parameterization given in (23) and (24) of [32], which was obtained by a fit to the result obtained in the chiral soliton model [29]. That parameterization is given for a factorization scale $\mu = 0.6$ GeV, and we use the leading-order evolution equations to evolve it up. Because of mixing we then need the D -term in the gluon GPD of the proton, which we take as zero at $\mu = 0.6$ GeV. Following [27] we take $\Lambda^{(3)} = 232$ MeV and $\Lambda^{(4)} = 200$ MeV for the scale parameter in α_S , switching from 3 to 4 flavors at $\mu = 1.5$ GeV. For $\mu^2 = 5$ GeV² we get

$$D(z) \approx -(1 - z^2) [2.9C_1^{3/2}(z) + 0.6C_3^{3/2}(z) + 0.2C_5^{3/2}(z)], \quad (41)$$

with Gegenbauer polynomials $C_n^{3/2}(z)$. Below, we will give estimates with and without the D -term contribution according to (40) and (41) in order to explore the model dependence of our results.

In Fig. 7 we show the real and imaginary parts of the convolution integral $\mathcal{H}_1(-\eta, \eta, t)$, calculated from H_{DD} . Decomposing $\mathcal{H}_1 = \mathcal{H}_1^u + \mathcal{H}_1^d + \mathcal{H}_1^s$ we plot the contributions from u , d , and s quarks separately. We further divide by appropriate factors $(1/2)F_1^u(t)$, $F_1^d(t)$, and $F_D(t)$, so that with the factorizing ansatz (34), (36) the resulting curves are independent of t ⁴. Analogous plots for $\tilde{\mathcal{H}}_1 = \tilde{\mathcal{H}}_1^u + \tilde{\mathcal{H}}_1^d$ are given in Fig. 8. We observe that for $\tau \sim 0.1$ the s quark contribution to $\text{Re}\mathcal{H}_1$ is by no means

⁴ Formally, these curves correspond to $\mathcal{H}_1^{u,d,s}$ at $t = 0$, which for $\tau \neq 0$ is however outside the physical region according to (13)

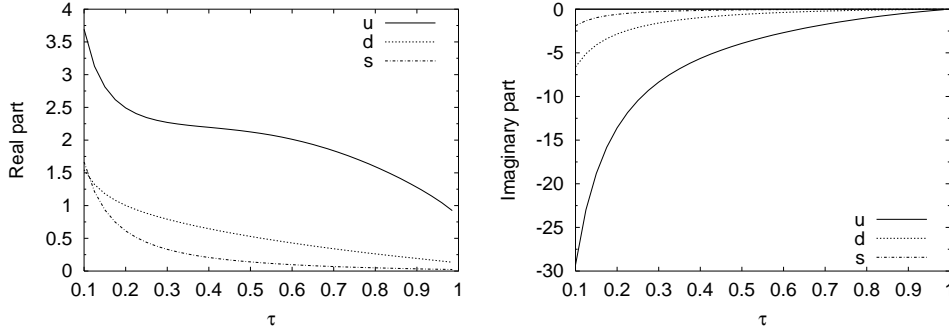


Fig. 7. The contributions from u , d , and s quarks to $\text{Re}\mathcal{H}_1$ (left) and $\text{Im}\mathcal{H}_1$ (right). They are calculated with $H^q = H_{\text{DD}}^q$ and respectively divided by $(1/2)F_1^u(t)$, $F_1^d(t)$, and $F_D(t)$

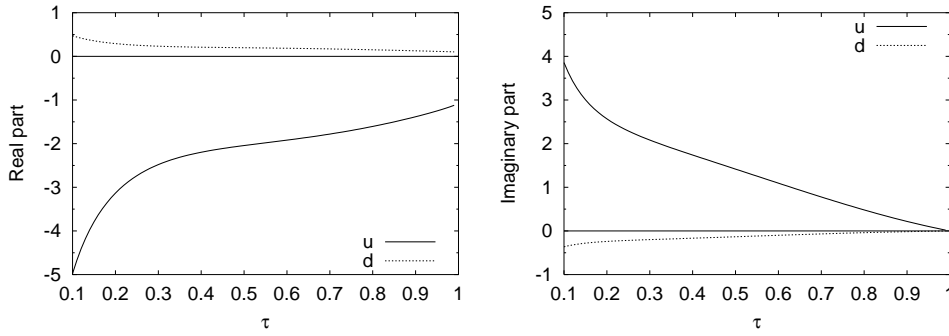


Fig. 8. The contributions from u and d quarks to $\text{Re}\tilde{\mathcal{H}}_1$ (left) and $\text{Im}\tilde{\mathcal{H}}_1$ (right). They are calculated with our model for \tilde{H}^q and divided by $\tilde{F}^q(t)$

small compared with u and d quarks, although it is tiny in $\text{Im}\mathcal{H}_1$. This illustrates that at least the real part of the Compton amplitude is not related in a straightforward manner with the usual parton densities at $x \sim \tau$, given that $s(x)$ only becomes comparable to $u(x)$ and $d(x)$ for x considerably below 0.1.

We do not show in Fig. 7 the contributions from H_D . They are only nonzero in the real part, summed over all flavors they amount to a τ independent contribution of $-3.3F_D(t)$ in \mathcal{H}_1 . The remarkable fact that the D -term contribution to the TCS amplitude is independent of η at fixed t remains true to all orders in perturbation theory. This is because due to general scaling properties the hard scattering kernel can be written as the leading-order one in (5) times a function of x/η . Comparing with Fig. 7 we see that the D -term has an appreciable impact on the value of $\text{Re}\mathcal{H}_1$ in our model. This is surprising if one compares the functions H_D and H_{DD} themselves. We show this for u quarks in Fig. 9, plotting only the charge conjugation even combination $H(x, \eta, t) - H(-x, \eta, t)$ that enters in Compton scattering. One can understand the strong amplification of a moderate change in the ERBL region of a GPD by observing that the real part in the convolutions (5) is a principal value integral, which involves large cancellations between the contributions from $|x| < \eta$ and $|x| > \eta$. Here is one of the reasons why measuring the real part of the Compton amplitude, in DVCS or in TCS, can provide unique information on generalized parton distributions.

5.2 Cross section and angular distributions

To calculate the TCS amplitude we start with the hadronic tensor (4), evaluated in the γp c.m. with the 3-axis in

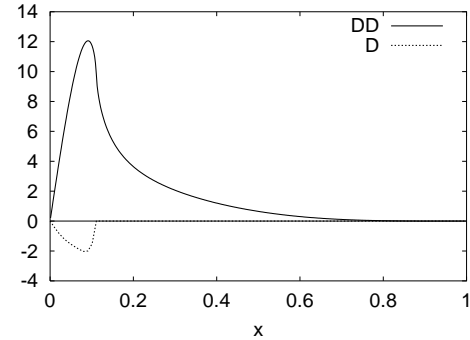


Fig. 9. The combination $H_{\text{DD}}^u(x, \eta, t) - H_{\text{DD}}^u(-x, \eta, t)$ divided by $(1/2)F_1^u(t)$, and the combination $H_D^u(x, \eta, t) - H_D^u(-x, \eta, t)$ divided by $F_D(t)$. Both curves are for $\eta = 0.11$, corresponding to $\tau = 0.2$

the direction of \vec{p} . In order to preserve gauge invariance beyond the leading-twist approximation, we use the prescription of [21] and take

$$T^{\alpha\beta} = T^{\alpha\gamma} \Big|_{\text{Eq. (4)}} \left(g_{\gamma}^{\beta} - q'_{\gamma} \frac{p'^{\beta}}{p'q'} \right), \quad (42)$$

where the index β refers to the virtual photon. The subtraction term is formally suppressed by $1/Q'$ and has effects of a few percent on the results we will present. The γp cross section is then calculated from (42) and the exact expression of the BH amplitude. We have compared the interference term thus obtained with the approximate expressions in Sect. 4.4. For $Q'^2 = 5 \text{ GeV}^2$, $|t| = 0.2 \text{ GeV}^2$, and $s^{1/2} = 5 \text{ GeV}$ we find that the approximation (30) with (33) deviates by at most 10% from what we obtain with (42). As one expects, the situation gets worse for

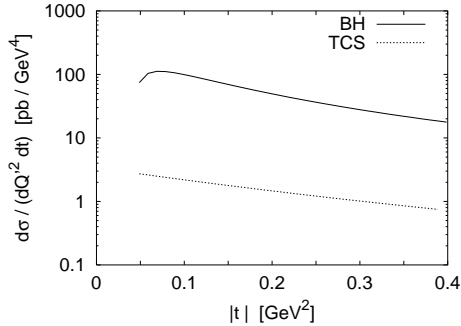


Fig. 10. The BH (solid line) and TCS (dotted line) cross sections for $s^{1/2} = 5 \text{ GeV}$ and $Q'^2 = 5 \text{ GeV}^2$, integrated over $\varphi \in [0, 2\pi]$ and $\theta \in [\pi/4, 3\pi/4]$. The TCS contribution is calculated using H_{DD}^q and \tilde{H}_{DD}^q from (34), (36)

larger values of $|t|$ but improves quickly for larger values of Q'^2 .

We are now ready to estimate the different contributions to the cross section. In Fig. 10 we show the result for the TCS and the BH contributions to the φ -integrated cross section at $s^{1/2} = 5 \text{ GeV}$ and $Q'^2 = 5 \text{ GeV}^2$. Here and in the following we integrate over θ from $\pi/4$ to $3\pi/4$, avoiding the region where the BH contribution becomes hopelessly large. As we anticipated in Sect. 4.3 the BH process nevertheless dominates the cross section, with TCS contributing less than 5% in this kinematics. In Fig. 10 there is no contribution from the interference between TCS and BH since the angular integration selects charge conjugation even quantities. Let us therefore investigate the manifestation of the interference term in the angular distribution. We restrict ourselves to unpolarized photons here.

In Fig. 11a we show the φ dependence of the cross section integrated over θ in the range $[\pi/4, 3\pi/4]$. With the integration limits symmetric about $\theta = \pi/2$ the interference term is odd under $\varphi \rightarrow \pi + \varphi$ due to charge conjugation, whereas the TCS and BH cross sections are even. We separately show the contribution from BH and the sum of BH and the interference term. The TCS cross section is flat in φ to leading-twist accuracy, cf. (25), and only tiny oscillations are induced by the prescription (42). In the kinematics of the figure we get $d\sigma_{\text{TCS}}/(dQ'^2 dt d\varphi) \approx 0.2 \text{ pb GeV}^{-4}$ when applying the same cut in θ and taking the double distribution ansatz (34) for the GPDs.

Figure 11b shows the corresponding contributions to the weighted cross section

$$\frac{dS}{dQ'^2 dt d\varphi} = \int_{\pi/4}^{3\pi/4} d\theta \frac{L(\theta, \varphi)}{L_0(\theta)} \frac{d\sigma}{dQ'^2 dt d\theta d\varphi}. \quad (43)$$

We see that the signal is more easily visible after this weighting. The interference term behaves now like $\cos \varphi$ up to $1/Q'$ suppressed terms that are numerically small. The weighted BH cross section is almost flat with our cut on θ , in line with our discussion at the end of Sect. 4.2. The TCS contribution is again small here and will not much change the picture. As discussed in Sect. 4.4, information on the interference can in principle also be obtained from

the φ -integrated cross section. With the same kinematics as in Fig. 11 we find that the interference generates an asymmetry in $d\sigma/(dQ'^2 dt d\theta)$ about $\theta = \pi/2$ which is barely at the 1% level.

To extract information on the Compton amplitude in a compact way we introduce

$$R = \frac{2 \int_0^{2\pi} d\varphi \cos \varphi \frac{dS}{dQ'^2 dt d\varphi}}{\int_0^{2\pi} d\varphi \frac{dS}{dQ'^2 dt d\varphi}}, \quad (44)$$

which projects out the ratio a_1/a_0 of Fourier coefficients in the weighted cross section $dS/(dQ'^2 dt d\varphi) = \sum_{n=0}^{\infty} a_n \cos(n\varphi)$. Up to $1/Q'$ suppressed contaminations the numerator in R is proportional to the combination \tilde{M}^{--} of Compton amplitudes, whereas the denominator is in our kinematics dominated by the BH part of the cross section. To explore the dependence of our estimates on the GPDs we compare in Fig. 12 the ratio R for the cases where H^q is taken from the double distribution ansatz (34), (36) alone, or as the sum of this and the D -term in (40). Due to a numerical accident the contributions from H_{DD} , H_{D} and \tilde{H}_{DD} in (33) nearly cancel each other and produce a quite small interference term. This result should be interpreted with care since, as we discussed, H_{DD}^q is obtained by extrapolating information from the usual parton distributions into the ERBL region, and our H_{D}^q is the result of a particular dynamical model. With a generic D -term of the same size one could also obtain a rather sizeable interference signal, as we see in Fig. 12 when combining H_{DD}^q and H_{D}^q with the “wrong” sign for H_{D}^q . In accordance with our discussion at the end of Sect. 5.1 we conclude from this exercise that the unpolarized interference term is highly sensitive to the behavior of the GPDs in the ERBL region, where our modeling is least reliable.

Figure 13 shows R for the same three models of H^q , now as a function of τ at fixed Q'^2 and t , and thus for varying collision energy $s^{1/2}$. Notice that at $\tau = 0.36$ the minimum value of $|t|$ is equal to 0.2 GeV^2 so that one is in collinear kinematics, where the angle φ is undefined. As the numerator of R projects out the coefficient of a $\cos \varphi$ -dependent term in the cross section, it must strictly vanish at that point. We remark that $\tau = 0.36$ is still far from its maximum value $\tau_{\text{max}} = (1 + 2M/Q')^{-1} = 0.54$, where the production threshold $s^{1/2} = Q' + M$ is reached for $Q'^2 = 5 \text{ GeV}^2$. It is interesting to note that in TCS the total collision energy at threshold is large, whereas in DVCS or in inclusive deep inelastic scattering one scans the resonance mass region down to the proton mass as x_{B} approaches its upper limit 1. While the straightforward application of leading-twist dominance seems dangerous in TCS at τ close to τ_{max} , this might be an interesting regime to study parton-hadron duality.

We finally wish to remark on TCS with a neutron target. In that case the BH process is suppressed due to the zero charge of the neutron. We can explicitly see this in the approximation (22), where the term in brackets involving the (typically large) factor $1/\tau^2$ goes with a combination

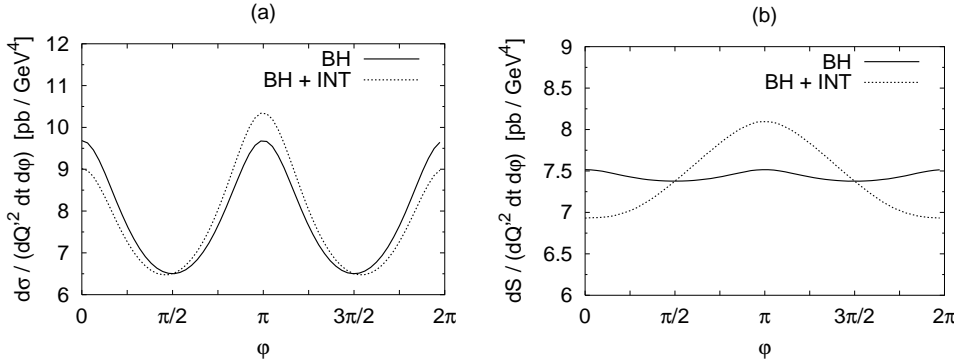


Fig. 11. **a** The cross section integrated over $\theta \in [\pi/4, 3\pi/4]$ as a function of φ for $s^{1/2} = 5 \text{ GeV}$, $Q^2 = 5 \text{ GeV}^2$, $|t| = 0.2 \text{ GeV}^2$. The curves represent the BH contribution (*solid line*) and the sum of BH and the interference term (*dash-dotted line*), calculated using H_{DD}^q and \tilde{H}_{DD}^q . **b** The same as in **a** but with the cross section weighted by L/L_0 before integrating over θ

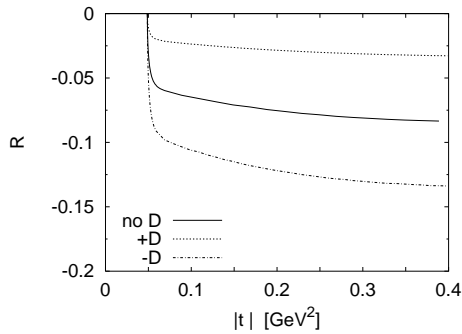


Fig. 12. The ratio R defined in (44) for $s^{1/2} = 5 \text{ GeV}$ and $Q^2 = 5 \text{ GeV}^2$. The curves correspond to the three models $H^q = H_{\text{DD}}^q$ (solid), $H^q = H_{\text{DD}}^q + H_{\text{D}}^q$ (dotted), and $H^q = H_{\text{DD}}^q - H_{\text{D}}^q$ (dash-dotted)

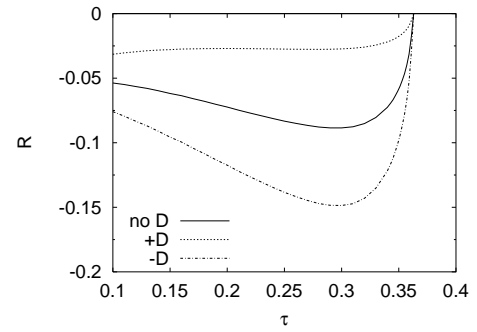


Fig. 13. The ratio R for the same models as in Fig. 12, but as a function of τ at $Q^2 = 5 \text{ GeV}^2$ and $|t| = 0.2 \text{ GeV}^2$

of form factors that vanishes for $t \rightarrow 0$. We find that the TCS contribution to the cross section is indeed more important than for a proton target. With the kinematics in Fig. 10 and the double distribution ansatz of (34) and (36) it does however not amount to much more than 10% of the BH contribution. The unpolarized interference term on the other hand generates a tiny ratio R of barely 1%. This can be understood from (33), where the potentially large contribution from \mathcal{H}_1 is suppressed by the Dirac form factor $\tilde{\mathcal{H}}_1$, whose prefactor survives in the $t \rightarrow 0$ limit, is penalized with a small factor η and further suppressed by a near cancellation of the charge-weighted polarized u and d quark densities in the neutron.

6 Summary and discussion

Next to DVCS, timelike Compton scattering may be the theoretically cleanest process where generalized parton distributions can be accessed. To leading twist and at Born level, both processes involve in fact the very same integrals over combinations of GPDs. At the level of α_s corrections and the departure from the large Q^2 limit, they will be different. A simultaneous description of both reactions may thus be a benchmark test of our understanding of the dynamics, both of the approximations employed in describing the parton-level process and of the nonperturbative input.

TCS can be measured in exclusive lepton pair production, either with quasi-real bremsstrahlung photons from incident leptons or with a dedicated real photon beam. Unlike DVCS, timelike Compton scattering is always accompanied by a Bethe–Heitler contribution much bigger than itself. It offers however relatively simple access to the real part of the Compton amplitude via the angular distribution of the produced lepton pair. Appropriate angular observables allow a rather clean investigation of the detailed structure of the Compton process. With circularly polarized incident photons one has access to the imaginary parts of the Compton amplitudes and thus to the timelike analog of what has been observed in the DVCS channel using the lepton spin asymmetry [33].

Using the quark handbag diagrams of Fig. 2 and simple models of the relevant GPDs we have estimated the cross section and angular asymmetries for lepton pair production in a kinematical setting typical of the HERMES regime. We find that the angular asymmetry carrying information on the Compton process ranges from about 5% to 15% within the variations of the GPD models we have explored. This rather wide range of predictions is generated by varying the GPDs in the ERBL region. It illustrates that the real part of the Compton amplitude is highly sensitive to the form of these distributions in the region where their physics is least known and most different from that of ordinary parton densities. Similar results have been obtained in recent studies of the lepton charge asymmetry in DVCS [32,34]. Given the uncertainties in modeling detailed features of GPDs, the numbers we estimate here should hence be taken with due care. We also

remark that substantial α_s corrections to the DVCS amplitude have been reported for our kinematics [35, 36]. In any case, whether the real part of TCS is observably large or not will already provide important information about the dynamics of the Compton process.

A look at (33) and the plots in Figs. 7 and 8 reveals that in the region of τ we considered, the imaginary part of the Compton amplitude is significantly larger than its real part. From (30) and (32) it then follows that in this kinematics the photon helicity asymmetry will be larger with our model GPDs than the unpolarized angular asymmetry we have investigated here.

We have not attempted to give estimates for the regime of very small τ , where DVCS has been observed at the HERA collider [37]. In that case, the contribution from gluon GPDs at order α_s is expected to be too important to be neglected. As to the Born level quark contribution below $\tau = 0.1$, we find in our model that as τ decreases both $\text{Re}\mathcal{H}_1$ and $-\text{Im}\mathcal{H}_1$ rise, as well as their ratio $-\text{Re}\mathcal{H}_1/\text{Im}\mathcal{H}_1$.

Contrary to what one might expect, our estimates for a neutron target do not give a much enhanced TCS signal in HERMES kinematics, neither in the cross section nor in the angular distribution. This is due to an unfortunate combination of mostly kinematic prefactors in the formulae for an unpolarized target. On the other hand, we do not expect such a suppression for coherent scattering on a deuteron target, whose GPDs have recently been discussed [38].

Acknowledgements. We gratefully acknowledge discussions with G. Anton, R. Baier, J. Blümlein, J. C. Collins, M. Düren, M. Fontannaz, A. Freund, T. Gousset, B. Kniehl, G. Kramer, M. McDermott, A. Meyer, M. Polyakov, B. Naroska, D. Schiff, and G. Sterman. This work is supported in part by the TMR and IHRP Programmes of the European Union, Contracts No. FMRX-CT98-0194 and No. HPRN-CT-2000-00130.

Appendix

In this appendix we discuss to which extent the evaluation of generalized parton distributions in the double distribution model (37) to (39) requires knowledge of the usual parton distributions down to $x = 0$. This is of practical importance since parton distributions are of course only constrained by data down to some finite value of x , below which one must rely on extrapolations.

As is well known, the terms in (37) going with $\delta(x-x'-\eta y')$ and $\delta(x+x'-\eta y')$ individually have non-integrable singularities at $x' = 0$, but their sum is finite. To make this explicit we consider the charge conjugation even combination $h_+(x, \eta) = h(x, \eta) - h(-x, \eta)$, which can be written as

$$h_+ \stackrel{x \leq \eta}{=} \int_0^{\frac{\eta-x}{(1+\eta)}} dx' \frac{q_+(x')}{\eta} \left[\pi \left(x', \frac{x-x'}{\eta} \right) - \pi \left(x', \frac{x+x'}{\eta} \right) \right] + \int_{\frac{\eta-x}{1+\eta}}^{\frac{\eta+x}{(1+\eta)}} dx' \frac{q_+(x')}{\eta} \pi \left(x', \frac{x-x'}{\eta} \right),$$

$$h_+ \stackrel{x \geq \eta}{=} \int_{\frac{x-\eta}{1-\eta}}^{\frac{\eta+x}{(1+\eta)}} dx' \frac{q_+(x')}{\eta} \pi \left(x', \frac{x-x'}{\eta} \right), \quad (45)$$

with $q_+(x) = q(x) + \bar{q}(x)$. Note that the corresponding singularities at $x' = 0$ are integrable for the quark valence combination $q(x') - \bar{q}(x')$, which is not needed in the evaluation of the Compton amplitude. The singularities for the polarized quark densities are integrable as well, and we can restrict our discussion to the most problematic case (45). Writing

$$\pi \left(x', \frac{x-x'}{\eta} \right) - \pi \left(x', \frac{x+x'}{\eta} \right) = \frac{3}{(1-x')^3} \frac{x-x'}{\eta}, \quad (46)$$

we see that the integrand in the first line of (45) only involves $x'q_+(x')$, whose singularity at $x' = 0$ is integrable.

The integrals in the second and third lines of (45) involve $q_+(x')$ down to values of order $x' \sim \eta - x$ and hence are potentially problematic for $x \rightarrow \eta$. To investigate them more closely, we decompose

$$\pi \left(x', \frac{x-x'}{\eta} \right) = \frac{3}{4(1-x'^3)} \times \left[\frac{x'(1-\eta)}{\eta} \frac{2\eta - \eta x' - x'}{\eta} + \frac{\eta - x}{\eta} \frac{\eta + x - 2x'}{\eta} \right]. \quad (47)$$

The first of the two terms in brackets leads again to the combination $x'q_+(x')$ and causes no trouble when the lower integration limit goes to zero as $x \rightarrow \eta$. The second term does not provide a factor x' but a factor $(\eta - x)$ instead. Let us for the sake of argument assume that for small x the quark density behaves like

$$xq_+(x) \sim x^{-\lambda} \quad (48)$$

with some $\lambda < 1$. For $x \rightarrow \eta$ the integral involving the second term in (47) then goes like

$$|\eta - x| \int_{|\eta-x|} dx' q_+(x') \stackrel{x \rightarrow \eta}{\sim} \frac{1}{\lambda} |\eta - x|^{1-\lambda} \quad (49)$$

and hence vanishes in the limit where its evaluation requires knowledge of $q_+(x')$ down to $x' = 0$.

To get a rough feeling for the integral in the first line of (45) and for the ones involving the first term in (47) let us consider $\int dx' x' q_+(x')$ with lower limit 0 and upper limit of order η . If we assume the power behavior (48), then the contribution from the interval $x' \in [0, \epsilon]$ to the total integral is of order $(\epsilon/\eta)^{1-\lambda}$. For typical values of λ this is about 10% if ϵ is one to two orders of magnitude smaller than η . Of course $q_+(x)$ is unknown below some value of x , but unless its small- x behavior is much steeper than (48), the above estimate should not be altered significantly.

Our discussion can be adapted to other profile functions $\pi(x', y')$ than the one in (39). Provided that $\pi(x', y')$ is differentiable in y' one can replace (46) with

$$\pi \left(x', \frac{x-x'}{\eta} \right) - \pi \left(x', \frac{x+x'}{\eta} \right) = -\frac{2x'}{\eta} \partial_2 \pi \left(x', \frac{x}{\eta} \right) + O(x'^2). \quad (50)$$

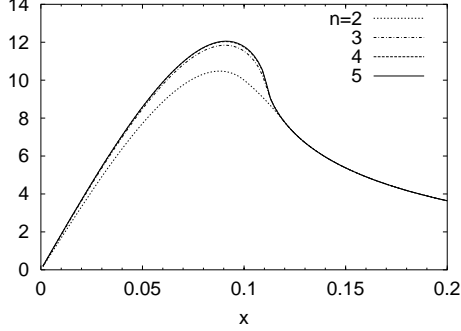


Fig. 14. $h_+^u(x, \eta)$ for $\eta = 0.11$, corresponding to $\tau = 0.2$, evaluated with a lower cutoff $\epsilon = 10^{-n}$ on x' in the integrals (45)

where $\partial_2\pi = \partial\pi(x', y')/\partial y'$. Decomposing

$$\frac{x-x'}{\eta} = (1-x') - \frac{x'(1-\eta)}{\eta} - \frac{\eta-x}{\eta} \quad (51)$$

we further see that (47) can be replaced with

$$\begin{aligned} & \pi\left(x', \frac{x-x'}{\eta}\right) \\ &= -\frac{x'(1-\eta)}{\eta} \partial_2\pi(x', 1-x') + O(x'^2) \\ & - \frac{\eta-x}{\eta} \partial_2\pi\left(x', 1-x' - \frac{x'(1-\eta)}{\eta}\right) + O((\eta-x)^2), \end{aligned} \quad (52)$$

provided again that $\pi(x', y')$ is differentiable in y' and that in addition $\pi(x', 1-x') = 0$.

Notice that while the GPD so obtained is finite at $x = \eta$, its first derivative in x is in general not. For profile functions $\pi(x', y')$ vanishing at $x' + y' = 1$ we readily obtain a representation of $\partial h_+/\partial x$ analogous to (45) with π replaced by $\eta^{-1}\partial_2\pi$. Provided that $\partial_2\pi$ is differentiable in y' our previous line of arguments goes through, except for the equivalents of (47) and (52). There one will have an extra term $\eta^{-1}\partial_2\pi(x', 1-x')$ on the right-hand side, which for our profile function (39) is nonzero. This means that the integrals corresponding to the second and third lines of (45) will have an integrand going like $q_+(x')$ at $x' \rightarrow 0$, without a factor $(\eta-x)$ in front. $\partial h_+/\partial x$ thus behaves for $x \rightarrow \eta$ like $\int dx' q_+(x')$ with lower limit of order $|\eta-x|$, and with the small- x behavior (48) diverges like

$$\left| \frac{\partial}{\partial x} h_+(x, \eta) \right| \stackrel{x \rightarrow \eta}{\sim} \frac{1}{\lambda} |\eta-x|^{-\lambda}. \quad (53)$$

Now, the principal value integral over x which gives $\text{Re}\mathcal{H}_1$ according to (5) effectively involves $\partial h_+/\partial x$ at x around η , but the singularity (53) is integrable and gives a finite result for the amplitude. One can also insert the expression (37) into (5) and explicitly carry out the integrals over x and y' for the profile function (39). The result for $\text{Re}\mathcal{H}_1$ has the form $\int_0^1 dx' x' q_+(x') \rho(x', \eta)$, where $\rho(x', \eta)$ has a $\log(x')$ singularity at $x' = 0$. Up to this logarithm the small- x' behavior of the quark density thus enters $\text{Re}\mathcal{H}_1$

in the same way as according to our above discussion it enters $h_+(\eta, \eta)$ and hence $\text{Im}\mathcal{H}_1$.

Let us explore how our arguments work at the quantitative level, restricting ourselves to u quarks for simplicity. In Fig. 14 we plot $h_+^u(x, \eta)$ at $\eta = 0.11$ as it is obtained from (45) when setting $u_+(x') = 0$ for x' below some cutoff ϵ . We find good convergence as ϵ approaches zero, the curves for $\epsilon = 10^{-4}$ and 10^{-5} being hardly distinguishable. All predictions in this paper have been obtained with $\epsilon = 10^{-5}$. Figure 15 shows $\text{Re}\mathcal{H}_1^u$ and $\text{Im}\mathcal{H}_1^u$ as functions of τ , calculated with the same cutoffs as in Fig. 14 when constructing the GPDs. Clearly the convergence is much slower for the real part, which can be traced back to large cancellations in the relevant integrals⁵. This illustrates again the sensitivity of $\text{Re}\mathcal{H}_1$ to small changes of the GPDs we have already encountered in Sect. 5.1.

In Fig. 16 we show $h_+^u(x, \eta)$ obtained from different parameterizations of the usual quark densities at $\mu^2 = 5 \text{ GeV}^2$, calculated with a lower cutoff $\epsilon = 10^{-5}$ on x' . We compare the GRV 94 LO parameterization used in our predictions with three NLO distributions in the $\overline{\text{MS}}$ scheme: GRV 94 NLO [27], GRV 98 NLO [39], and MRSA' [40]. All input densities are clearly distinct for x below 0.01, but above $x \approx 0.05$ the three NLO parameterizations hardly differ among themselves. The corresponding curves for $h_+^u(x, \eta)$ at $\eta = 0.11$ are almost identical for the NLO parameterizations, in accordance with our arguments about the relevance of small x in the input densities. In Fig. 17 we make the same comparison for $\text{Re}\mathcal{H}_1^u$ and $\text{Im}\mathcal{H}_1^u$. In line with our previous findings, differences between the parameterizations are more prominent for $\text{Re}\mathcal{H}_1^u$, but they remain quite small. Our results are compatible with those of [36, 41], where very similar GPDs and Compton amplitudes have been obtained from the GRV 98 NLO and MRSA' distributions with the same ansatz (37), (39) we have used here.

In summary, we have discussed in detail the calculation of GPDs with the double distribution ansatz (37). In the DGLAP region the calculation of $h_+(x, \eta)$ involves the usual quark densities down to $x' = (x-\eta)/(1-\eta)$, whereas in the ERBL region the ansatz literally does require knowledge of $q_+(x')$ down to $x' = 0$. The corresponding integrals involve however only the combination $x'q_+(x')$, or they vanish like (49). The contribution from $q_+(x')$ at values of x' several orders of magnitude below η should thus be moderate, unless one has an extremely steep rise of the quark density at small x' . We confirm this

⁵ For the numerical evaluation of (5) we add and subtract $H(x, \eta, t)$ at the points $|x| = \eta$. To avoid cancellations as much as possible we only do this for $|x| < 2\eta$ when $\eta < 1/2$, writing

$$\begin{aligned} & \text{PV} \int_0^1 dx \left[\frac{1}{x-\eta} - \frac{1}{x+\eta} \right] h_+(x, \eta) \\ &= \int_0^{2\eta} dx \left[\frac{1}{x-\eta} - \frac{1}{x+\eta} \right] [h_+(x, \eta) - h_+(\eta, \eta)] \\ & + h_+(\eta, \eta) \ln \frac{1}{3} + \int_{2\eta}^1 dx \left[\frac{1}{x-\eta} - \frac{1}{x+\eta} \right] h_+(x, \eta), \end{aligned}$$

where PV denotes the principal value prescription

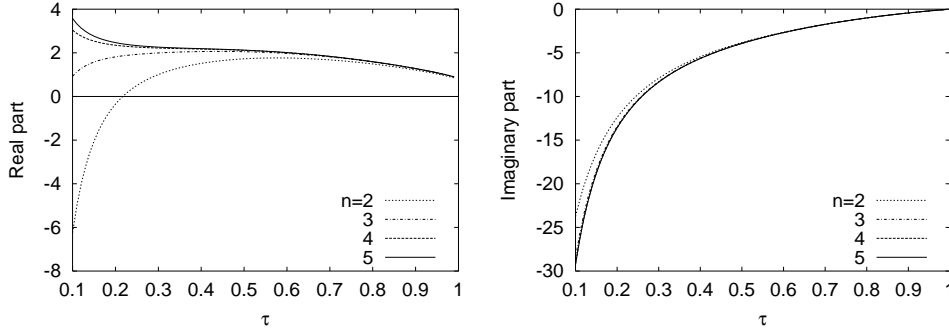


Fig. 15. $\text{Re}\mathcal{H}_1^u$ (left) and $\text{Im}\mathcal{H}_1^u$ (right) divided by $\frac{1}{2}F_1^u(t)$, calculated from the GPDs in Fig. 14

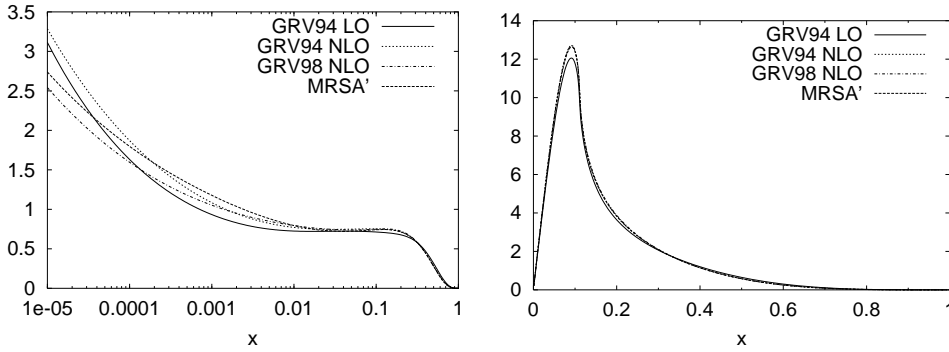


Fig. 16. Left: Different parameterizations of $u(x) + \bar{u}(x)$ for $\mu^2 = 5 \text{ GeV}^2$. Right: The corresponding generalized distributions $h_+^u(x, \eta)$ at $\eta = 0.11$, obtained with our double distribution ansatz

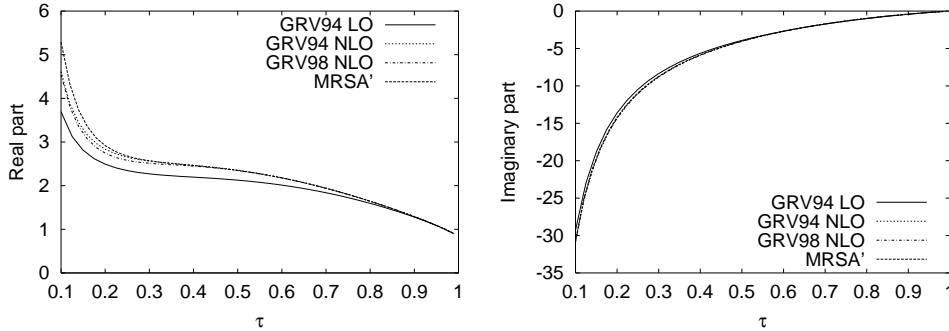


Fig. 17. $\text{Re}\mathcal{H}_1^u$ (left) and $\text{Im}\mathcal{H}_1^u$ (right) divided by $\frac{1}{2}F_1^u(t)$, calculated from the same parameterizations of $u(x) + \bar{u}(x)$ as in Fig. 16

numerically by evaluating the integrals (45) with different lower cutoffs on x' . For η of order 0.1 we find rather similar GPDs when implementing the ansatz (37) with different parameterizations of the quark densities, given that they show only mild discrepancies down to x' of order 10^{-2} .

The derivative of $h_+(x, \eta)$ at $x \rightarrow \eta$ becomes infinite with the profile function we used in our double distribution ansatz, but the corresponding singularity in x is integrable. The small- x behavior of $q_+(x)$ is found to affect the real and imaginary parts of the Born level Compton amplitude in a similar way, with the real part showing somewhat higher sensitivity. Again we confirmed this in our numerical study.

We finally emphasize that our discussion of how relevant the usual quark densities at very small x are in the construction of GPDs refers to a particular *model* prescription. It is a different question to what extent one *physically* expects the behavior of $q_+(x)$ at $x \rightarrow 0$ to be reflected in GPDs at finite η . In the representation of GPDs as the overlap of wave functions for the incoming and outgoing hadron [42] one finds indeed that for $x \rightarrow \eta$ a quark momentum in *one* of the two wave functions goes to zero.

This is similar to, but not the same as the situation for a usual quark density at $x \rightarrow 0$, where *both* wave functions involve a quark with zero momentum.

References

1. D. Müller, D. Robaschik, B. Geyer, F.M. Dittes, J. Hořejši, Fortsch. Phys. **42**, 101 (1994) [hep-ph/9812448]; J. Blümlein, B. Geyer, D. Robaschik, Nucl. Phys. B **560**, 283 (1999) [hep-ph/9903520]
2. X. Ji, Phys. Rev. Lett. **78**, 610 (1997) [hep-ph/9603249]
3. A.V. Radyushkin, Phys. Rev. D **56**, 5524 (1997) [hep-ph/9704207]
4. J.C. Collins, A. Freund, Phys. Rev. D **59**, 074009 (1999) [hep-ph/9801262]
5. J.C. Collins, private communication
6. A.V. Belitsky, D. Müller, L. Niedermeier, A. Schäfer, Nucl. Phys. B **593**, 289 (2001) [hep-ph/0004059]
7. A.V. Belitsky, A. Freund, D. Müller, Nucl. Phys. B **574**, 347 (2000) [hep-ph/9912379]
8. L. Mankiewicz, G. Piller, E. Stein, M. Vanttinen, T. Weigl, Phys. Lett. B **425**, 186 (1998) [hep-ph/9712251]

9. M. Diehl, T. Gousset, B. Pire, J.P. Ralston, Phys. Lett. B **411**, 193 (1997) [hep-ph/9706344]
10. P. Hoodbhoy, X. Ji, Phys. Rev. D **58**, 054006 (1998) [hep-ph/9801369]; A.V. Belitsky, D. Müller, Phys. Lett. B **486**, 369 (2000) [hep-ph/0005028]; M. Diehl, Eur. Phys. J. C **19**, 485 (2001) [hep-ph/0101335]
11. I.V. Anikin, B. Pire, O.V. Teryaev, Phys. Rev. D **62**, 071501 (2000) [hep-ph/0003203]; M. Penttinen, M.V. Polyakov, A.G. Shuvaev, M. Strikman, Phys. Lett. B **491**, 96 (2000) [hep-ph/0006321]; A.V. Belitsky, D. Müller, Nucl. Phys. B **589**, 611 (2000) [hep-ph/0007031]; N. Kivel, M.V. Polyakov, A. Schäfer, O.V. Teryaev, Phys. Lett. B **497**, 73 (2001) [hep-ph/0007315]; A.V. Radyushkin, C. Weiss, Phys. Rev. D **63**, 114012 (2001) [hep-ph/0010296]
12. N. Kivel, L. Mankiewicz, hep-ph/0106329
13. G. Parisi, Phys. Lett. B **90**, 295 (1980)
14. J.C. Collins, L. Frankfurt, M. Strikman, Phys. Rev. D **56**, 2982 (1997) [hep-ph/9611433]
15. W.J. Stirling, M.R. Whalley, J. Phys. G **19**, D 1 (1993)
16. J. Badier et al. [NA3 Collaboration], Phys. Lett. B **142**, 446 (1984); K. Freudenreich, Int. J. Mod. Phys. A **5**, 3643 (1990)
17. J.Z. Bai et al. [BES Collaboration], hep-ex/0102003
18. M.L. Swartz, Phys. Rev. D **53**, 5268 (1996) [hep-ph/9509248]
19. K. Schilling, P. Seyboth, G.E. Wolf, Nucl. Phys. B **15**, 397 (1970)
20. P. Kroll, M. Schürmann, P.A.M. Guichon, Nucl. Phys. A **598**, 435 (1996) [hep-ph/9507298]
21. P.A. Guichon, M. Vanderhaeghen, Prog. Part. Nucl. Phys. **41**, 125 (1998) [hep-ph/9806305]
22. S. Boffi, C. Giusti, F.D. Pacati, Phys. Rept. **226**, 1 (1993)
23. L.A. Ahrens et al., Phys. Rev. D **35**, 785 (1987)
24. M. Penttinen, M.V. Polyakov, K. Goeke, Phys. Rev. D **62**, 014024 (2000) [hep-ph/9909489]
25. M. Diehl, T. Feldmann, R. Jakob, P. Kroll, Eur. Phys. J. C **8**, 409 (1999) [hep-ph/9811253]; S.J. Brodsky, M. Diehl, D.S. Hwang, Nucl. Phys. B **596**, 99 (2001) [hep-ph/0009254]; B.C. Tiburzi, G.A. Miller, hep-ph/0104198
26. I.V. Musatov, A.V. Radyushkin, Phys. Rev. D **61**, 074027 (2000) [hep-ph/9905376]
27. M. Glück, E. Reya, A. Vogt, Z. Phys. C **67**, 433 (1995)
28. T. Gehrmann, W.J. Stirling, Phys. Rev. D **53**, 6100 (1996) [hep-ph/9512406]
29. V.Y. Petrov, P.V. Pobylitsa, M.V. Polyakov, I. Börnig, K. Goeke, C. Weiss, Phys. Rev. D **57**, 4325 (1998) [hep-ph/9710270]
30. B. Pire, J. Soffer, O. Teryaev, Eur. Phys. J. C **8**, 103 (1999) [hep-ph/9804284]
31. M.V. Polyakov, C. Weiss, Phys. Rev. D **60**, 114017 (1999) [hep-ph/9902451]
32. N. Kivel, M.V. Polyakov, M. Vanderhaeghen, Phys. Rev. D **63**, 114014 (2001) [hep-ph/0012136]; K. Goeke, M.V. Polyakov, M. Vanderhaeghen, hep-ph/0106012
33. A. Airapetian et al. [HERMES Collaboration], Phys. Rev. Lett. (in press) [hep-ex/0106068]; S. Stepanyan et al. [CLAS Collaboration], hep-ex/0107043
34. V.A. Korotkov, W.D. Nowak, hep-ph/0108077
35. A.V. Belitsky, D. Müller, L. Niedermeier, A. Schäfer, Phys. Lett. B **474**, 163 (2000) [hep-ph/9908337]
36. A. Freund, M.F. McDermott, hep-ph/0106319
37. C. Adloff et al. [H1 Collaboration], Phys. Lett. B **517**, 47 (2001) [hep-ex/0107005]; J.C. Hart [ZEUS Collaboration], hep-ex/0108023
38. E.R. Berger, F. Cano, M. Diehl, B. Pire, Phys. Rev. Lett. **87**, 142302 (2001) [hep-ph/0106192]
39. M. Glück, E. Reya, A. Vogt, Eur. Phys. J. C **5**, 461 (1998) [hep-ph/9806404]
40. A.D. Martin, W.J. Stirling, R.G. Roberts, Phys. Lett. B **354**, 155 (1995) [hep-ph/9502336]
41. A. Freund, M.F. McDermott, hep-ph/0106115
42. S.J. Brodsky, M. Diehl, D.S. Hwang, Nucl. Phys. B **596**, 99 (2001) [hep-ph/0009254]; M. Diehl, T. Feldmann, R. Jakob, P. Kroll, Nucl. Phys. B **596**, 33 (2001) [Erratum-ibid. B **605**, 647 (2001)] [hep-ph/0009255]